Complete Experimental Structure Determination of the p(3×2)pg Phase of Glycine on Cu{110}

Zhasmina V. Zheleva, Tugce Eralp, and Georg Held*

Department of Chemistry, The University of Reading, Whiteknights, UK

E-mail: g.held@reading.ac.uk

October 23, 2011

Abstract

We present a quantitative low energy electron diffraction (LEED) surface-crystallograpic study of the complete adsorption geometry of glycine adsorbed on Cu{110} in the ordered $p(3\times2)$ phase. The glycine molecules form bonds to the surface through the N atoms of the amino group and the two O atoms of the de-protonated carboxylate group, each with separate Cu atoms such that every Cu atom in the first layer is involved in a bond. Laterally, N atoms are nearest to the atop site (displacement 0.41 Å). The O atoms are asymmetrically displaced from the atop site by 0.54 Å and 1.18 Å with two very different O-Cu bond lengths of 1.93 Å and 2.18 Å. The atom positions of the upper-most Cu layers show small relaxations within 0.07 Å of the bulk-truncated surface geometry. The unit cell of the adsorbate layer consists of two glycine molecules, which are related by a glide-line symmetry operation. This study clearly shows that a significant coverage of adsorbate structures without this glide-line symmetry must be rejected, both on the grounds of the energy dependence of the spot intensities (LEED-IV curves) and of systematic absences in the LEED pattern.

Keywords:

Glycine, Amino Acids, Copper, Low Energy Electron Diffraction (LEED)

*To whom correspondence should be addressed

Introduction

The interactions between small organic molecules, such as amino acids and other carboxilic acids, and metal surfaces have been of interest for many years, both because of their biological importance and their implications for heterogeneous chemical reactions. Metal surfaces catalyse a range of chemical modifications, e.g. (de)hydrogenation, oxidation, decomposition, polymerization, but also structural modifications of the metal substrates have been observed, which are suspected to play a significant role in the chiral modification of heterogeneous catalysts.[1–5] Glycine is the simplest of the amino acids and thus a convenient model for chemisorption of amino acids in general. In this context, the adsorption of glycine on Cu{110} has received particular attention. The system has been studied experimentally using photoelectron spectroscopy and diffraction (XPS, PhD), near-edge X-ray adsorption (NEXAFS), low energy electron diffraction (LEED), scanning tunneling microscopy (STM) and IR spectroscopy,[6–13] and by DFT ab-initio calculations.[14–17] All these studies concluded a similar adsorption structure for the most stable chemisorbed species, glycinate, which involves a de-protonated carboxylate group and bonds to surface Cu atoms through the two O atoms of the carboxylate group and the N atom of the amino group, as shown in Figure 1.a, but a complete experimental structure determination is still missing. An asymmetric "triangular footprint" is a common feature of small amino acids adsorbed on Cu{110} and other Cu surfaces.[17–23] Since glycine itself is not chiral, two adsorption geometries are possible, which are mirror images of each other and are, therefore, referred to as "enantiomers" in the text (Figure 1.b shows a structure with both enantiomers). In the absence of lateral interactions the two geometries are energetically equal and should therefore occur with the same probability.

At saturation of the chemisorbed layer, glycinate forms a $p(3\times2)$ overlayer with two molecules in the unit cell, as confirmed by STM.[10] A question that has been debated in the recent literature is, whether the surface layer of glycine consists of an equal mixture of "homochiral" domains, each consisting only of one type of enantiomer, or "heterochiral" domains, where neighbouring molecules are opposite enantiomers. The LEED pattern of the $p(3\times2)$ superstructure after annealing to 400 K shows systematic absence of the $(0,\ \pm(n+\frac{1}{2}))$ spots, which indicates a unit

cell with a glide line (*pg* space group) and, hence, a heterochiral structure with mirror images of molecules (i.e. opposite enantiomers) displaced by half a lattice constant with respect to each other, as shown in Figure 1.b.[12] However, based on the observation of two distinct domains in their STM experiments Chen et al.[10] suggested that homochiral as well as heterochiral domains coexist on the Cu {110} surface. A model for the homochiral domains has been suggested in which the glycine molecules within the unit cell are laterally displaced by a vector $\frac{3}{2}\vec{a}_1 + \vec{a}_2$ as shown in Figure 1.d. Theoretical studies favor a homochiral arrangement but have also found other homochiral structures, different from the one above,[15,16] which have only slightly higher adsorption energies than the heterochiral structure so that a maximum of 15% of the surface area could be covered by molecules in such arrangements. In these models (cf. Figure 1.c) the glycine molecules are slightly rotated with respect to each other and have, therefore, different local geometries and bonding sites. Since there is no mirror operation relating the two molecules in the homochiral models glide-plane symmetry is not possible. It has been argued, however, that the difference between the geometry models of Figure 1.b,c,d is only due to weak scatterers such as C, N and O atoms. If the footprints of the molecules in the homochiral structures would still constitute a glide-line symmetry this could, therefore, still lead to near extinction of the missing spots.[1,10]

Here we present a quantitative LEED-IV study, which yields, for the first time, a complete set of structural parameters derived from experiment including all atomic positions of the adsorbate (except hydrogen) and the topmost Cu layers. We find a clear preference for the heterochiral model and show that the dynamically calculated intensities of the "missing spots" for homochiral structures would be of the same order of magnitude as the observed spots. A heterochiral footprint arrangement alone is, therefore, not sufficient to explain the systematic extinctions in the LEED pattern. Instead, the molecular layer must have true glide-plane symmetry.

Experimental and Computational Methods

Experiment

The experiments were carried out in an ultrahigh vacuum (UHV) chamber equipped with sputter gun, quadrupole mass spectrometer for temperature programmed desorption (TPD) measurements, and a low-current micro channel-plate (MCP) LEED instrument (Omicron NanoTechnology). The sample temperature was measured through a thermocouple attached to the sample holder plates.

Standard procedures such as argon ion sputtering (5 μA, 600V for 20 min) and annealing to 1000 K were used to clean the sample in UHV.[24] Glycine (Sigma-Aldrich, purity $> 99\%$) was deposited from a glass tube placed in a stainless steel crucible, which was resistively heated to 403 K. The evaporator was mounted behind a gate valve allowing control of the deposition time.

During deposition the sample was held at a temperature around 315 K in order to suppress the formation of multilayers. Typical deposition times required to achieve a saturated chemisorbed layer were around 30 min. Subsequent annealing to 400 K led to a sharp $p(3 \times 2)$ LEED pattern. LEED images were recorded with the sample at room temperature using the MCP-LEED in combination with a standard Video-LEED acquisition system. The energy range was between 30 and 250 eV, in steps of 1 eV, and the primary electron beam current was kept in the 10 nA range. No significant changes in the the LEED intensities of the glycine superstructure were observed over a period of 30 min. The typical total exposure time for collecting a complete set of LEED images is of the order of 10 min, which corresponds to a total exposure of about 7 electrons per glycine molecule, given a beam diameter of 1 mm. This is low enough to avoid significant beam damage. Experimental data was taken for two different angles of incidence, which correspond to an azimuthal rotation of about 60° at a polar angle of 5° off the surface normal. Taking data for two angles of incidence increases the data set and, hence, the accuracy of the analysis.[25,26] The LEED patterns showed systematic absences of the $(0,\pm(n+\frac{1}{2}))$ spots for all energies, as reported previously.[10,12] A total of 24 inequivalent IV curves were extracted for both angles of incidence with a cumulative energy range of 1953 eV. The spot intensities were extracted from the LEED im-

ages using our MKIV program,[27] which determines the positions of all spots simultaneously and records their intensities even if they cannot be resolved from the background. The extracted IV curves were processed using Fourier transform smoothing to eliminate the high-frequency noise.

Each LEED experiment was followed by a TPD experiment, measuring the partial pressures of the main decomposition products, H_2 and CO_2, in order to confirm the coverage.

LEED calculations

The structure determination was performed with our fully automated "CLEED" program[28] package which was modified such that it is able to analyze LEED-IV data taken at different angles of incidence simultaneously. This program package employs fully dynamical scattering theory along the lines of algorithms developed by Pendry[29] and Van Hove / Tong.[30] Bulk scattering was calculated by Pendry's layer doubling method with bulk inter-layer spacings of 1.28 Å for Cu{110}. Convergence is typically achieved by including 32 bulk layers. The downhill simplex method was used for optimizing the structural parameters and the exact angles of incidence.[31] The agreement between the experimental and theoretical IV curves was quantified with Pendry's R_P factor and the error limits for the determined parameters were calculated using the *RR* factor method.[32] The cumulative energy overlap of 1953 eV in the present analysis leads to a *RR* factor of 13%. The scattering phase shifts for all atoms within the structure were calculated as a function of energy using the program package provided by Barbieri and Van Hove.[33] The hydrogen atoms were ignored in the LEED calculations as it is common practice. The maximum angular momentum quantum number l_{max} was 8. For the imaginary and real part of the potential 4.0 eV and -10 eV, respectively, were used in accordance with earlier work on Cu{110}.[34,35] The Debye temperature was kept at bulk value (343 K) for all Cu atoms, which corresponds to a radial root mean square (rms) displacement of 0.03 Å. For the O, N and C atoms constant rms displacement values of 0.10 Å were used in accordance with earlier work.[25,26]

The existence of domains with different orientations poses a fundamental problem when using off-normal angles of incidence. Whenever the overlayer unit cell has a lower symmetry than the

bulk-terminated surface domains of energetically degenerate molecular orientations should coexist in equal numbers within the area sampled by the electron beam. If interference between the domains can be neglected the observed LEED pattern is a superposition of the patterns originating from each domain. This affects integer and fractional order spots. For normal incidence the LEED IV curves of all domains can be derived from one calculation for a single domain by applying the respective mirror and/or rotation operations to the pattern emerging from this domain and averaging the IV curves of overlapping spots accordingly. If the angle of incidence differs from the surface normal (and is outside a mirror plane), however, each domain has a different orientation with respect to the incoming electron beam and, hence, separate calculations have to be performed for each domain and the intensities have to be averaged accordingly if the spot positions overlap in reciprocal space. This is a non-trivial problem and increases the computer time required for the data analysis significantly. Individual R_P factors were calculated by comparing the domain-averaged calculated IV-curves with the experimental data set for each angle of incidence. The overall R_P factor, which is used for the structure optimization, is a weighted average over all angles of incidence whereby the relative contribution of each angle depends on the cumulative energy range used for calculating the individual R_P value.

We have performed structural optimization of the three models presented in Figure 1.b,c,d. The heterochiral model (Figure 1.b) shares the $[001]$ mirror/glide plane with the substrate but not the two-fold rotation symmetry; therefore the average of two domains has to be taken into account. The homochiral models (Figure 1.c,d) have neither a mirror plane nor rotational symmetry, which leads to four possible domains.

Results

The optimization process was divided into two steps. First the z-distance of the Cu atoms in the first two layers and the position of the glycine molecules were optimized. In the second step all coordinates of the atoms in the two glycine molecules and the coordinates of the Cu atoms in the

top-most three layers were optimized. For all models the start geometry for the Cu substrate was bulk-truncated.

The initial geometry for the heterochiral structure was the same as the geometry suggested in the DFT study by Rankin and Sholl.[16] It remains unchanged upon a reflection with respect to the [001] mirror plane (dotted line in Figure 1.b) followed by a translation by the vector $\vec{a}_2 = \frac{1}{2}\vec{b}_2$, which constitutes a glide-line operation. During the optimization process, symmetry-equivalent atoms in the substrate and overlayer were only allowed to move in accordance with these symmetry constraints (equivalent Cu atoms of the first and second layer are labeled in Figure 1.b), which restricts the number of geometry parameters. The *x*,*y*,*z* coordinates of the first two Cu layers and the *z*-coordinates of the third layer were optimized. Together with the atomic coordinates of the glycine molecules this leads to 36 structural parameters that were optimized in the final stage.

The two homochiral models are depicted in Figure 1.c and d. The initial geometry for model I (Figure 1.c) was the one suggested in the DFT study by Rankin and Sholl.[16] The homochiral structure model II (Figure 1.d) is that suggested in the STM study by Chen et al.[36] Its start geometry had one molecule in the same position as in the heterochiral structure and the second molecule shifted by half a superstructure unit-cell vector in both directions with respect to the first (Figure 1.d). This leads to different bonding sites for the O atoms of the two molecules. None of the homochiral structures has a true glide line symmetry. Therefore the number of independent structural parameters is greater. In order to keep the total number of parameters within a reasonable limit for the homochiral structures only the *z*-coordinates of the topmost three Cu layers (42 parameters in total) were optimized.

The lowest R_P-factors found for the heterochiral model and the homochiral models I and II were 0.22 ,0.28 and 0.27, respectively. The two homochiral models lie well outside the statistical error margin of the R_P factor minimum for the the heterochiral structure ($\Delta R_P = RR \cdot R_{P,min} = 0.03$), therefore the LEED-IV analysis clearly favours the heterochiral model. In addition, both best-fit geometries found for the homochiral models were not physically reasonable in terms of bond lengths and angles within the glycine molecules. The coordinates of the best-fit geometry

for the heterochiral model are listed in Table 1; for better comparability, derived parameters, such as displacements, bond lengths, and bond angles are listed in Table 2 and compared with results from previous studies. To illustrate the agreement between calculated and experimental LEED-IV curves representative examples are plotted in Figure 2.

Discussion

Our analysis provides the first complete experimental structure determination of any amino acid on a metal surface. In this special case of glycine on Cu{110} it confirms that the adlayer does, indeed, form a heterochiral structure. The best-fit geometry consists of glycine molecules forming three bonds with separate copper atoms. The two oxygen atoms differ in their positions relative to the nearest Cu atoms. They are displaced from the atop site along the [001] direction by δ_y[O(1)] = 0.53 Å and δ_y[O(2)] = 1.12 Å, respectively (the total lateral displacements, δ_{tot}, are 0.54 Å and 1.18 Å). In the $[1\bar{1}0]$ direction the O atoms are slightly displaced towards each other, which brings them closer to the O-O distance in the gas-phase carboxylic group (2.33 Å vs 2.25 Å in the gas phase), and their vertical heights differ by 0.09 Å, following the corrugation of the underlying Cu atoms. The different lateral displacements from the atop sites lead to significantly different Cu-O bond lengths of Cu(1)–O(1) = 1.93 Å and Cu(2)–O(2) = 2.18 Å. The N atom of the amino group is on the same side as the O(1) atom. The displacements of the N atom from the atop site are smaller than for the oxygen atoms (δ_x[N] = 0.32 Å; δ_y[N] = 0.25 Å; δ_{tot}[N] = 0.41 Å) and close to the error bars for lateral displacements. The Cu(3)–N bond length is 2.04 Å. All molecular displacements and bond lengths are in good quantitative agreement with the values determined previously by PhD[8,11] and the more recent total energy calculations by Rankin and Sholl[16,17] (cf. Table 2).

The the O-O axis of the two inequivalent oxygen atoms is tilted by α[O(1)–O(2)] = 13° with respect to the row of close-packed Cu atoms ($[1\bar{1}0]$). This is between the values determined by NEXAFS,[6] 25°, and DFT,[16] 6°. The C(1)-C(2) backbone is essentially parallel to the [001] di-

rection (tilted by 6°) and the angle between the plane defined by the carboxylic group and surface plane, α[O(1)-C(1)-O(2)], is 42°, which is, again, in good agreement with the aforementioned DFT and NEXAFS studies, which report α[O(1)-C(1)-O(2)] values of 36° and 30°, respectively. The intramolecular bond lengths derived from the LEED-IV analysis are also listed in Table 2 and compared with the DFT results[16] and the gas-phase values for the zwitterionic form of glycine.[37] the DFT and LEED values agree within 0.06 Å or less for all bond lengths, except C(2)–N, for which the discrepancy is more than 0.2 Å. Tabulated values for single C–N bond lengths in gas-phase molecules range from 1.32 Å (diazomethane) to 1.48 Å (diazirine),[38] therefore neither of the two values, 1.31 Å (LEED) or 1.52 Å, can be considered unphysical. The intermolecular distances between O(1) and O(2) and the nitrogen atoms of the neighbouring molecules are 2.9 Å, which is within the range of strong hydrogen bonds.[39] Stabilization of the glycinate layer through hydrogen bonds was suggested in the theoretical studies by Nyberg et al. and Rankin and Sholl.[15,16]

All Cu atoms of the first substrate layer are involved in a bond to the adsorbate. The biggest height difference (0.07 Å) is between the two inequivalent Cu atoms which form oxygen bonds. The copper atoms of the first three layers show small relaxation shifts of less than 0.07 Å with respect to the bulk-truncated positions. The average contraction of the first layer, $\Delta d_{1,2}$, is 0.03 Å and the average vertical deviations of the second and third layer from their bulk values are less than 0.02 Å (cf Table 1). Previous LEED-IV studies of the clean Cu{110} surface found larger relaxations up to $\Delta d_{1,2} = 0.11$ Å,[35,40] but our findings agree with the general observation that adsorption of molecules reverses the inward relaxation observed for most clean metal surfaces.

So far, our conclusion that the glycine adlayer is assuming a heterochiral structure was entirely based on the comparison of the IV curves of observable spots in the LEED pattern. The fact that the $(0, \pm(m + \frac{1}{2}))$ spots are missing is another very strong argument in favour of the heterochiral vs a homochiral structure because only the former can have a true a glide line symmetry.[12] It has been argued by several authors, however, that an approximate glide-line symmetry, where only a few light atoms violate the symmetry, would also lead to the systematic extinction - or at least substantial weakening - of the respective spots.[10,18] Chen et al. have performed a kinematic

calculation, which only considered the adsorbate atoms of the homochiral structure proposed in Ref.[10] (cf Figure 1.d). This led to missing spots at the $(\pm\frac{2n-1}{3}, \pm m)$ and $(\pm\frac{2n}{3}, \pm(m+\frac{1}{2}))$ positions, which is equivalent to a $c(3\times 2)$ LEED pattern. For the heterochiral structure the spots at the $(0, \pm(m+\frac{1}{2}))$ positions are missing due to the glide-line. The authors concluded that the superposition of the LEED patterns from the two domain types would lead to the observed pattern with missing spots only at the $(0, \pm(m+\frac{1}{2}))$ positions and explain the fact that two domains were seen in the STM images. However, the homochiral structure in Figure 1.d does not have a true centered unit cell, since the two molecules have different registry with the substrate, which is not accounted for in the kinematic calculations. In Figure 3, we present dynamical LEED-IV calculations for one representative missing spot, $(0, \frac{1}{2})$, for the best-fit geometries of all three models studied in the present investigation (cf Figure 1.b,c,d). The IV curves of the missing spots were not used in the structure determination because no experimental data are available. Nevertheless, the fact that they are not observed is an important piece of information. Figure 3.a shows a comparison of the relative intensities of the $(0, \frac{1}{2})$ spot for the three models. Note that the IV-curve for the heterochiral model is exactly zero (within numerical errors), as expected from the glide-line symmetry, whereas the curves for the two homochiral models are comparable with other fractional order spots (for comparison, the $(\frac{2}{3}, \frac{1}{2})$ IV curve of the heterochiral model is also included in the Figure). The unscaled, background-corrected experimental IV curves of the two spots, the missing $(0, \frac{1}{2})$ and the observed $(\frac{2}{3}, \frac{1}{2})$, are plotted in Figure 3.b. No features greater than the average noise level can be detected in the $(0, \frac{1}{2})$ IV curve. The noise level is about 20 times lower than the average intensity of the $(\frac{2}{3}, \frac{1}{2})$ spot. Therefore, the heterochiral model is the only one that matches the experimental observations. This is not in contradiction to the STM images of Chen et al.[10] since even a pure heterochiral $p(2\times 3)$ structure would be expected to exist in two mirror domains. The clean Cu{110} surface has a mirror-plane along the $[1\bar{1}0]$ direction, therefore, the structure shown in Figure 1.c and its mirror image with respect to $[1\bar{1}0]$ ($\vec{a}_1$) should cover equal areas of the surface. An asymmetric STM tip could easily lead to different appearances of these two domains, as observed in Ref.[10] Note also that four mirror/rotation domains would coexist in a homochiral

superstructure (see above). Therefore, a mixed homochiral/heterochiral overlayer should lead to the observation of six domains in STM.

An interesting question in this context is how a small deviation from the true glide-line symmetry would affect the intensity of the missing spots. For this purpose we have carried out intensity calculations for a modified heterochiral model where the central C(2') atom of one of the two molecules is shifted in steps of 0.05 Å along the $[1\bar{1}0]$ direction away from its symmetric position. The results for the $(0, \frac{1}{2})$ beam are shown in Figure 3.b. Although C is a weak scatterer and LEED is usually not very sensitive to lateral shifts, even a slight violation of the glide plane symmetry, by 0.05 Å already leads to significant intensity in the missing spots. For a shift of 0.10 Å intensity should be measurable at least at certain energies; it and can therefore be excluded. Moving the C atom by 0.20 Å makes the intensity already comparable to the other fractional order beams, e.g. the $(\frac{2}{3}, \frac{1}{2})$ in Figure 3.a, which is plotted at the same scale. The difference in the x-coordinate of the central C atom is around 0.7 Å between the homochiral and heterochiral DFT models, which explains the large theoretical intensity for the homochiral model I. On the basis of our experimental data we can exclude any deviations greater than 0.1 Å from the glide-line symmetry, which is significantly smaller than most of the error bars associated with other lateral coordinates of the adsorbate. These considerations demonstrate that systematic absences in an experimental LEED pattern imply very strict symmetry constraints. Even small deviations from these symmetries or small areas covered by other structures violating the symmetry would make the "missing spots" observable. The fluctuations in the experimental $(0, \frac{1}{2})$ curve in Figure 3.c would only be compatible with a relative area of less than 5% covered with a homochiral minority species.

Summary

In summary we have carried out a full LEED-IV structural analysis of the $p(3 \times 2)$ overlayer of glycine on Cu{110}, which shows systematic absences in the diffraction pattern. The unit cell of the adsorbate layer consists of two glycine molecules, which are related by a glide-line operation.

The molecules bind to the surface through the N atom of the amino group and the two O atoms of the de-protonated carboxylate group, each forming a bond with a separate Cu atom. The N atom is nearest to the atop site (lateral displacement 0.41 Å). The O atoms are further displaced from the atop site by 0.54 Å and 1.18 Å with two very different O-Cu bond lengths of 1.93 Å and 2.18 Å. The atom positions of the upper-most Cu layers show small relaxations within 0.07 Å of the bulk-truncated surface geometry. A quantitative analysis of calculated intensities for the spots that are systematically absent in the experimental LEED patters reveals that any structural model that violates a glide-line symmetry by shifts of more than about 0.1 Å must be rejected.

Acknowledgement

ZVZ acknowledges a postgraduate studentship grant from the ”Research Endowment Trust Fund” of the University of Reading. The authors would also like to thank D. Sholl for making the full data set of Ref.[16] available.

References

(1) Barlow, S. M.; Raval, R. *Surf. Sci. Rep.* **2003**, *50*, 201–341.

(2) Baddeley, C. *Top. Catal.* **2003**, *25*, 17–28.

(3) Held, G.; Gladys, M. J. *Top. Catal.* **2008**, *48*, 128–136.

(4) Ma, Z.; Zaera, F. *Surf. Sci. Rep.* **2006**, *61*, 229–281.

(5) Baddeley, C. J.; Held, G. In *Chiral Molecules on Surfaces*, 1st ed.; Andrews, D., G., S., G., W., Eds.; Comprehensive Nanoscience and Technology; Elsevier: Amsterdam, 2010; pp 105–133.

(6) Hasselström, J.; Karis, O.; Weinelt, M.; Wassdahl, N.; Nilsson, A.; Nyberg, M.; Petterson, L. G. M.; Samant, M. G.; Stöhr, J. *Surf. Sci.* **1998**, *407*, 221–236.

(7) Hasselstrom, J.; Karis, O.; Nyberg, M.; Pettersson, L.; Weinelt, M.; Wassdahl, N.; Nilsson, A. *J. Phys. Chem. B* **2000**, *104*, 11480–11483.

(8) Booth, N. A.; Woodruff, D. P.; Schaff, O.; Gießel, T.; Lindsay, R.; Baumgärtel, P.; Bradshaw, A. M. *Surf. Sci.* **1998**, *397*, 258–264.

(9) Barlow, S. M.; Kitching, K. J.; Haq, S.; Richardson, N. V. *Surf. Sci.* **1998**, *401*, 322–335.

(10) Chen, Q.; Frankel, D. J.; Richardson, N. V. *Surf. Sci.* **2002**, *497*, 37–46.

(11) Kang, J.-H.; Toomes, R. L.; Polcik, M.; Kittel, M.; Hoeft, J.-T.; Efstathiou, V.; Woodruff, D. P.; Bradshaw, A. M. *J. Chem. Phys.* **2003**, *118*, 6059–6071.

(12) Toomes, R. L.; Kang, J.-H.; Woodruff, D. P.; Polcik, M.; Kittel, M.; Hoeft, J.-T. *Surf. Sci. Lett.* **2003**, *522*, L9–L14.

(13) Shavorskiy, A.; Aksoy, F.; Grass, M. E.; Liu, Z.; Bluhm, H.; Held, G. *J. Am. Chem. Soc.* **2011**, *133*, 6659–6667.

(14) Nyberg, J., M. Hasselström; Karis, O.; Wassdahl, N.; Weinelt, M.; Nilsson, A.; Petterson, L. G. M. *J. Chem. Phys.* **2000**, *112*, 5420–5427.

(15) Nyberg, M.; Odelius, M.; Nilsson, A.; Petterson, L. G. M. *J. Chem. Phys.* **2003**, *119*, 12577–12585.

(16) Rankin, R. B.; Sholl, D. S. *Surf. Sci.* **2004**, *548*, 301–308.

(17) Rankin, R. B.; Sholl, D. S. *J. Phys. Chem. B* **2005**, *109*, 16764 – 16773.

(18) Barlow, S. M.; Louafi, S.; Le Roux, D.; Williams, J.; Muryn, C.; Haq, S.; Raval, R. *Surf. Sci.* **2005**, *590*, 243–263.

(19) Rankin, R. B.; Sholl, D. S. *J. Chem. Phys.* **2006**, *124*, 074703–1–6.

(20) Jones, G.; Jones, L. B.; Thibault–Starzyk, F.; Seddon, E. A.; Raval, R.; Jenkins, S. J.; Held, G. *Surf. Sci.* **2006**, *600*, 1924–1935.

(21) Eralp, T.; Zheleva, Z. V.; Shavorskiy, A.; Dhanak, V. R.; Held, G. *Langmuir* **2010**, *26*, 10918–10923.

(22) Eralp, T.; Shavorskiy, A.; Zheleva, Z. V.; Held, G.; Kalashnyk, N.; Ning, Y.; Linderoth, T. R. *Langmuir* **2010**, *26*, 18841–18851.

(23) Eralp, T.; Shavorskiy, A.; Held, G. *Surf. Sci.* **2011**, *605*, 468–472.

(24) Ammon, C.; Bayer, A.; Steinrück, H. P.; Held, G. *Chem. Phys. Lett* **2003**, *377*, 163–169.

(25) Held, G.; Wander, A.; King, D. A. *Physical Review B (Condensed Matter)* **1995**, *51*, 17856–17866.

(26) Braun, W.; Held, G. *Surf. Sci.* **2005**, *594*, 203–211.

(27) Held, G.; Uremovic, S.; Stellwag, C.; Menzel, D. *Rev. Sci. Instr.* **1996**, *67*, 378.

(28) Held, G.; Braun, W. CLEED manual. available from the authors.

(29) Pendry, J. B. *Low Energy Electron Diffraction*; Academic Press: London, 1974.

(30) Van Hove, M. A.; Tong, S. Y. *Surface Crystallography by LEED*; Springer Series in Solid–State Sciences; Springer: Berlin, 1979.

(31) Press, W. H.; Flannery, B. P.; Teukolsky, S. A.; Vetterling, W. T. *Numerical Recipes in C*; Cambridge University Press: Cambridge, 1988.

(32) Pendry, J. B. *J. Phys. C: Solid State Phys.* **1980**, *13*, 937–944.

(33) Barbieri, A.; Van Hove, M. A. Phase shift program package. available from http://electron.lbl.gov/software/software.html.

(34) Davis, H.; Noonan, J.; Jenkins, L. *Surface Science* **1979**, *83*, 559 – 571.

(35) Davis, H.; Noonan, J. *Surface Science* **1983**, *126*, 245–252.

(36) Chen, Q.; Richardson, N. V. *Annual Rep. Prog. Chem., Sect. C* **2004**, *100*, 313–347.

(37) Oegerle, W. R.; Sabin, J. R. *Journal of Molecular Structure* **1973**, *15*, 131–136.

(38) Lide, D. R.; Frederikse, H. P. R. *Handbook of Chemistry and Physics*, 76th ed.; CRC Press: Boca Raton, 1995.

(39) Jones, G.; Jenkins, S. J.; King, D. A. *Surf. Sci.* **2006**, *600*, L224–L228.

(40) Noonan, J. R.; Davis, H. L.; Jenkins, L. H. *Journal of Vacuum Science and Technology* **1978**, *15*, 619–621.

Table 1: Geometry parameters of the best fit structure for Cu{110}-$p(3\times2)$-glycinate. For comparison, the coordinates of the bulk-terminated Cu{110} surface are also listed. All coordinates are given in Å; coordinates with no error margins are related through symmetry to another atom within the same layer (glycine overlayer and layers 1 to 3) or not optimized (layer 4). See Figure 1.a for the labels of atoms; symmetry-related atoms are indicated by primes; the error margins refer to all symmetry-related atoms. *rmsd* = root mean square displacement due to thermal vibrations, $\Delta d_{n,n+1}$ = average vertical deviation from bulk-terminated geometry.

		bulk termination			Cu{110}-$p(3\times2)$-Gly				
		x	*y*	*z*	*rmsd*	*x*	*y*	*z*	$\Delta d_{n,n+1}$
1st Gly	O(1)	-0.05	0.70	1.82	0.1	-0.22 (±0.24)	0.56 (±0.21)	1.85 (±0.06)	
molecule	O(2)	2.24	0.95	1.82		2.05 (±0.23)	1.09 (±0.29)	1.76 (±0.05)	
	N	0.32	3.70	2.08		0.43 (±0.23)	3.45 (±0.36)	1.97 (±0.11)	
	C(1)	1.05	1.30	2.16		0.87 (±0.23)	1.18 (±0.26)	2.12 (±0.10)	
	C(2)	0.91	2.60	2.95		0.87 (±0.20)	2.59 (±0.24)	2.84 (±0.07)	
2nd Gly	O(1')	5.20	4.34	1.82	0.1	5.33	4.17	1.85	
molecule	O(2')	2.91	4.59	1.82		3.06	4.70	1.76	
	N'	4.83	7.34	2.08		4.68	7.06	1.97	
	C(1')	4.09	4.94	2.16		4.23	4.79	2.12	
	C(2')	4.24	6.24	2.95		4.24	6.20	2.84	
1st Cu	Cu(1)	0.00	0.00	0.00	0.03	-0.12 (±0.20)	0.02 (±0.16)	0.00 (±0.08)	-0.04
layer	Cu(2)	2.55	0.00	0.00		2.42 (±0.20)	-0.04 (±0.20)	-0.07 (±0.07)	
	Cu(3)	5.11	0.00	0.00		5.00 (±0.19)	0.09 (±0.18)	-0.04 (±0.07)	
	Cu(1')	5.11	3.61	0.00		5.22	3.63	0.00	
	Cu(2')	2.55	3.61	0.00		2.68	3.57	-0.07	
	Cu(3')	0.00	3.61	0.00		0.11	3.70	-0.04	
2nd Cu	Cu(4)	1.28	1.81	-1.28	0.03	1.43 (±0.21)	1.87 (±0.28)	-1.27 (±0.09)	0.00
layer	Cu(5)	3.83	1.81	-1.28		3.99 (±0.19)	1.85 (±0.20)	-1.27 (±0.05)	
	Cu(6)	6.38	1.81	-1.28		6.36 (±0.16)	1.76 (±0.22)	-1.31 (±0.07)	
	Cu(4')	3.83	5.42	-1.28		3.68	5.48	-1.27	
	Cu(5')	1.28	5.42	-1.28		1.12	5.46	-1.27	
	Cu(6')	6.38	5.42	-1.28		6.40	5.37	-1.31	
3rd Cu	Cu(7)	0.00	0.00	-2.55	0.03	0.00	0.00	-2.60 (±0.10)	0.02
layer	Cu(8)	2.55	0.00	-2.55		2.55	0.00	-2.50 (±0.11)	
	Cu(9)	5.11	0.00	-2.55		5.11	0.00	-2.49 (±0.11)	
	Cu(7')	5.11	3.61	-2.55		5.11	3.61	-2.60	
	Cu(8')	2.55	3.61	-2.55		2.55	3.61	-2.50	
	Cu(9')	0.00	3.61	-2.55		0.00	3.61	-2.49	
Cu	Cu	1.28	1.81	-3.83	0.03				
bulk									

1st angle of incidence $\theta_1 = 4.6^\circ$ $\phi_1 = 270^\circ$ $\Delta E_1 = 1230eV$ $RR_1 = 0.16$ $R_{p_1} = 0.19$
2nd angle of incidence $\theta_2 = 6.2^\circ$ $\phi_2 = 330^\circ$ $\Delta E_2 = 723eV$ $RR_2 = 0.21$ $R_{p_2} = 0.26$
Total $\Delta E = 1953eV$ $RR = 0.13$ $R_p = 0.22$

Table 2: Comparison of structural parameters derived from the LEED-IV analysis of Cu{110}-$p(3\times2)$-glycine and from previous experimental and theoretical studies on the same system and the gas-phase structure of the glycine zwitterion. All coordinates are given in Å and angles in degrees. α[O(1)–C(1)–O(2)] is the angle between the COO triangle and the surface; α[O(1)–O(2)] is the angle formed by the O-O axis and the $[1\bar{1}0]$ direction. The parameters $\delta_{x/y}$ refer to the displacement from the atop site; they are defined in Figure 1.a; the total lateral displacement, δ_{tot}, is defined as $\sqrt{\delta_x^2+\delta_y^2}$.

Parameter	**LEED-IV**	**PhD**[11]	**DFT**[16]	**NEXAFS**[6]	**gas phase**[37]
Nitrogen					
δ_x[N]	0.32 ($\pm$0.30)	0.24 ($\pm$0.10)	0.21		
δ_y[N]	0.25 ($\pm$0.40)	0.00 ($\pm$0.15)	0.09		
δ_{tot}[N]	0.41 ($\pm$0.35)				
d[Cu(3)-N]	2.04 ($\pm$0.15)	2.04 ($\pm$0.02)	2.11		
Oxygen O(1)					
δ_x[O(1)]	0.11 ($\pm$0.31)	0.08 (-0.08/+0.22)	-0.02		
δ_y[O(1)]	0.53 ($\pm$0.26)	0.68 ($\pm$0.09)	0.72		
δ_{tot}[O(1)]	0.54 ($\pm$0.28)				
d[Cu(1)-O(1)]	1.93 ($\pm$0.12)	2.02 ($\pm$0.04)	2.01		
Oxygen O(2)					
δ_x[O(2)]	0.37 ($\pm$0.30)	0.22 (-0.22/+0.18)	-0.30		
δ_y[O(2)]	1.12 ($\pm$0.35)	0.97 $\pm$0.08	0.96		
δ_{tot}[O(2)]	1.18 ($\pm$0.32)				
d[Cu(2)–O(2)]	2.18 ($\pm$0.17)	2.00 $\pm$0.04	2.10		
Substrate Bond Angles					
α[O(1)–C(1)–O(2)]	42°($\pm$17°)		36°	30° (35°)	
α[O(1)–O(2)]	13°($\pm$8°)	7°	6°	25°	
Intramolecular Bond Lengths					
d[O(1) – O(2)]	2.33		2.30		2.25
d[C(1) – O(1)]	1.29		1.31		1.30
d[C(1) – O(2)]	1.23		1.29		1.30
d[C(1) – C(2)]	1.58		1.52		1.47
d[C(2) – N]	1.31		1.52		1.45

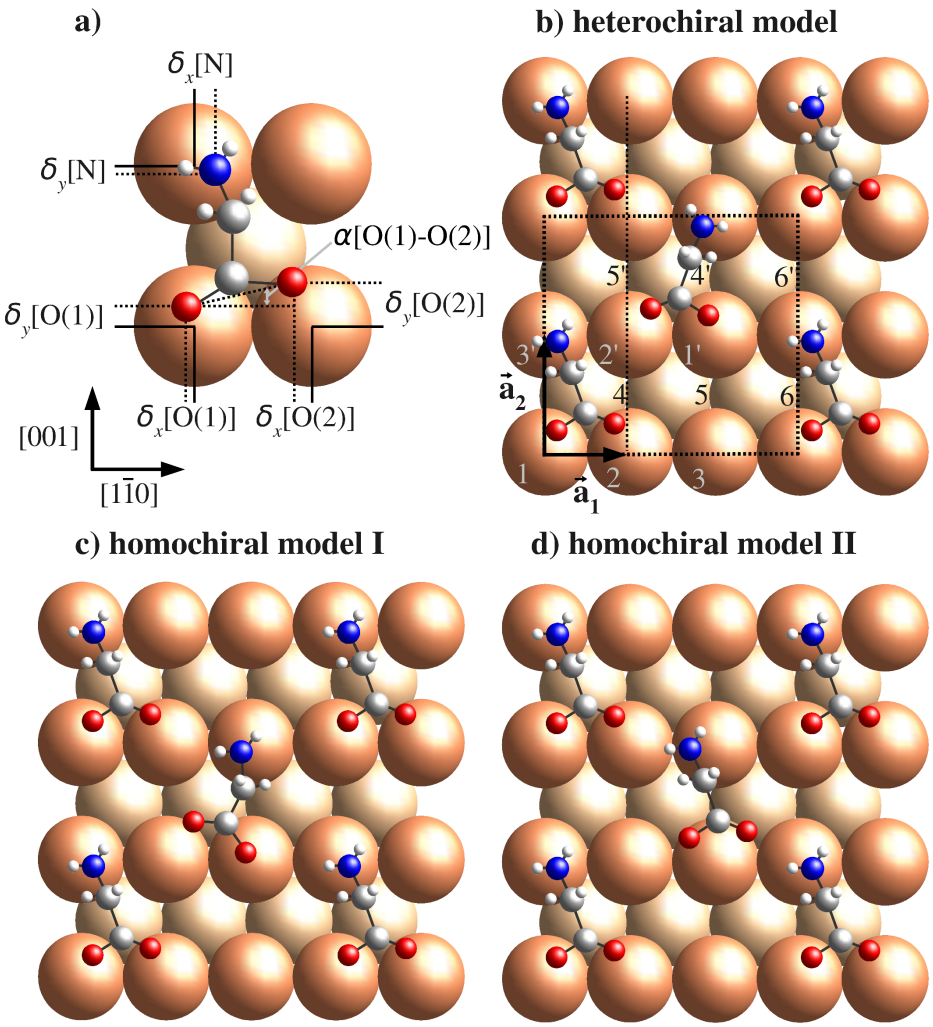

Figure 1: Schematic drawings of the model structures of glycinate overlayers on Cu{110}: a) a plan view of the best-fit structure; some of the structural parameters used in Table 2 are indicated; b) heterochiral model, in which the unit cell has a glide-line, indicated by the dotted line; c) homochiral model I suggested by DFT;[15–17] d) homochiral model II based on the structure proposed by Chen et al.;[10] models c) and d) do not have glide-line symmetry.

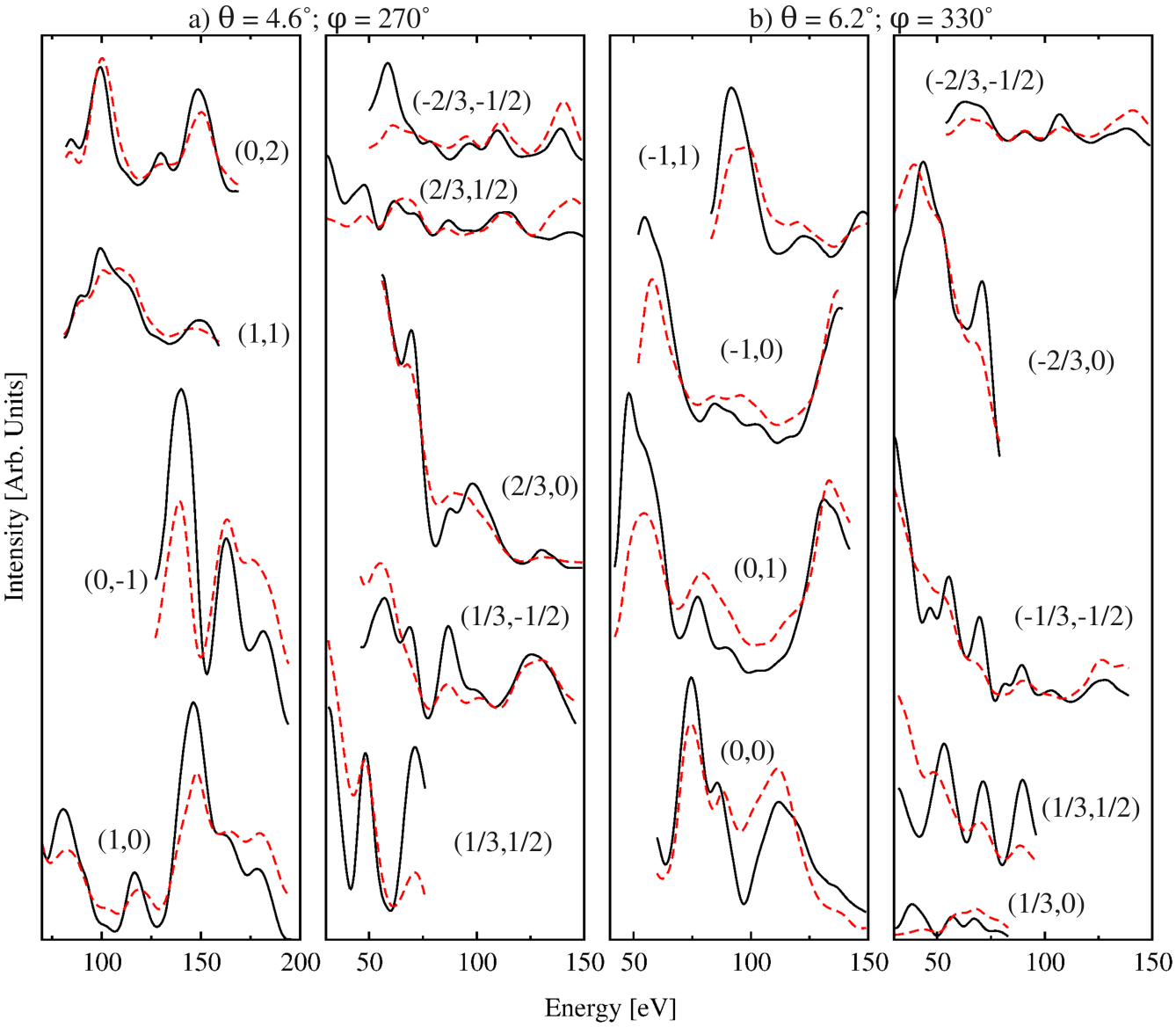

Figure 2: Selected representative experimental (black) and theoretical (red) LEED-IV curves for the best-fit structure of the heterochiral model.

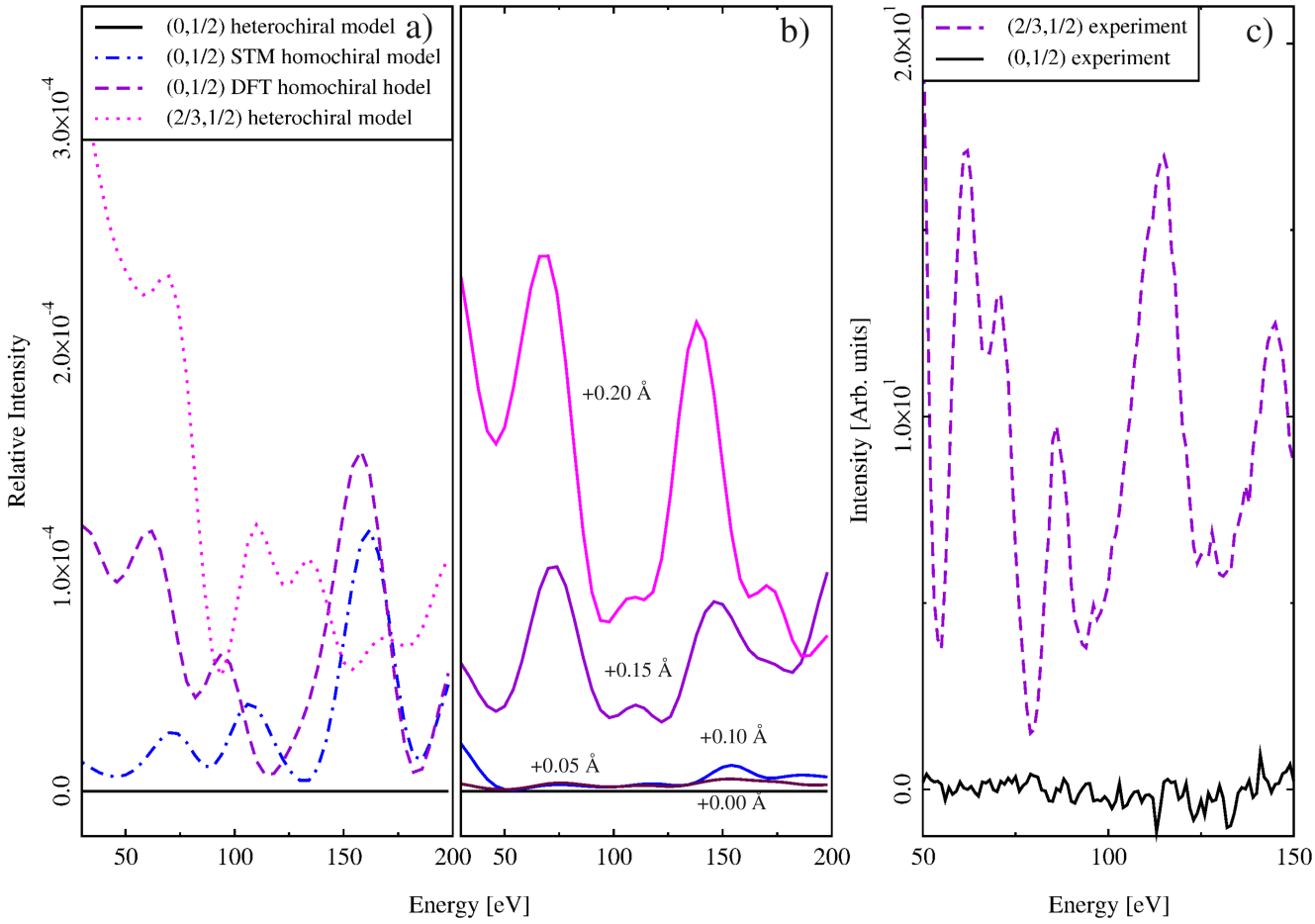

Figure 3: a) LEED-IV curves from dynamic calculations for the $(0, \frac{1}{2})$ beam of the homochiral and heterochiral models shown in Figure 1.b,c,d and for the $(\frac{2}{3}, \frac{1}{2})$ beam of the heterochiral model; b) experimental IV curves of the $(0, \frac{1}{2})$ and $(\frac{2}{3}, \frac{1}{2})$ beams. c) calculated IV curves for the $(0, \frac{1}{2})$ beam from the heterochiral overlayer (Figure 1.b) whereby the C(2') atom is shifted along the $[1\bar{1}0]$ direction by the distance indicated in the Figure. These calculations were performed for normal incidence.

TOC Graphics